

Orbital Parameters for the Soft X-ray Transient 4U 1543-47: Evidence for a Black Hole

Jerome A. Orosz¹

Department of Astronomy & Astrophysics, The Pennsylvania State University, 525 Davey Laboratory, University Park, PA 16802-6305
orosz@astro.psu.edu

Raj K. Jain^{1,2} and Charles D. Bailyn³

Department of Astronomy, Yale University, P.O. Box 208101, New Haven, CT 06520-8101
raj.jain@yale.edu, bailyn@astro.yale.edu

Jeffrey E. McClintock

Harvard-Smithsonian Center for Astrophysics, 60 Garden Street, Cambridge, MA 02138-1516
jem@cfa.harvard.edu

and

Ronald A. Remillard

Center for Space Research, Massachusetts Institute of Technology, Cambridge, MA 02139-4307
rr@space.mit.edu

ABSTRACT

Spectroscopic observations of the soft X-ray transient 4U 1543-47 reveal a radial velocity curve with a period of $P = 1.123 \pm 0.008$ days and a semi-amplitude of $K_2 = 124 \pm 4$ km s⁻¹. The resulting mass function is $f(M) = 0.22 \pm 0.02 M_\odot$. We classify the secondary star as A2V, in agreement with previous work, and measure $T_{\text{eff}} = 9000 \pm 500$ K and $E(B - V) = 0.50 \pm 0.05$ from fits to synthetic spectra. We derive a distance of $d = 9.1 \pm 1.1$ kpc if the secondary is on the main sequence. We see no emission lines from the accretion disk, and the measured fraction of disk light in the B and V bands is 10% and 21% respectively. The V and I light curves exhibit two waves per orbital cycle with amplitudes ≈ 0.08 mag. We modeled the light curves as ellipsoidal variations in the secondary star and derive extreme inclination limits of $20 \leq i \leq 40^\circ$. The formal 3σ limits on the inclination from a simultaneous fit to the V and I light curves are $24 \leq i \leq 36^\circ$ for a mass ratio $Q \equiv M_1/M_2 \geq 1$. However, there are systematic effects in

¹Visiting Astronomer at Cerro Tololo Inter-American Observatory (CTIO), which is operated by the Association of Universities for Research in Astronomy Inc., under contract with the National Science Foundation.

²Also Department of Physics, Yale University

³National Young Investigator

the data that the model does not account for, so the above constraints should be treated with caution. We argue that the secondary star is still on the main sequence with the mass transfer being driven by expansion due to normal main sequence evolution. If the secondary star has a mass near the main sequence values for early A-stars ($2.3 \leq M_2 \leq 2.6 M_\odot$), then the best fits for the 3σ inclination range ($24 \leq i \leq 36^\circ$) and the 3σ mass function range ($0.16 \leq f(M) \leq 0.28 M_\odot$) imply a primary mass in the range $2.7 \leq M_1 \leq 7.5 M_\odot$. The mass of the compact object in 4U 1543-47 is likely to be in excess of $\approx 3 M_\odot$, which is widely regarded as the maximum mass of a stable neutron star. Thus we conclude 4U 1543-47 most likely contains a black hole.

Subject headings: binaries: spectroscopic — black hole physics — X-rays: stars — stars: individual (4U 1543-47)

1. Introduction

4U 1543-47 is a bright soft X-ray transient that was observed in outburst in 1971 (Matilsky et al. 1972; Li et al. 1976), 1983 (Kitamoto et al. 1984), and 1992 (Harmon et al. 1992). This object is considered by many to be a strong black hole candidate based on its X-ray spectrum, which is composed of an ultra-soft component and a hard power-law tail (Tanaka & Lewin 1995).

The optical counterpart (IL Lup) was discovered shortly after the 1983 outburst (Pederson 1983). In quiescence the counterpart turned out to be unusual in several ways. For example Chevalier (1989) reported that the counterpart had faded by only 1.8 mag in V , much less than the ≈ 7 mag typical for soft X-ray transients (van Paradijs & McClintock 1995). Also, the spectral type of the secondary was A2V, much earlier than the usual K-type stars found in systems like A0620-00 or Nova Mus 1991. Finally, Chevalier noted that the spectrum of the quiescent counterpart lacked emission lines of any kind, whereas one expects to see strong Balmer emission lines from an accretion disk (van Paradijs & McClintock 1995). Chevalier did not state whether any photometric variability or radial velocity variations were observed. He proposed three hypotheses to explain the A2V star at the position of 4U 1543-47: a) The A star is in the line of sight to the X-ray source and not physically associated with it; b) The A star is a very “unusual” mass donor star; c) The A star is the outer star of a triple system with a low-mass X-ray binary as the inner pair.

GRO J1655-40, an important X-ray transient, was discovered in 1994 (Zhang et al. 1994). The optical counterpart of this source (V1033 Sco) has some characteristics similar to those of the counterpart of 4U 1543-47. First, the optical outburst amplitude was a modest 3.3 mag in V (Bailyn et al. 1995a). In addition, the secondary is an early type star (F5 IV, Bailyn et al. 1995b; Orosz & Bailyn 1997a, hereafter OB97). Finally, the optical spectrum of GRO J1655-40 in X-ray quiescence is devoid of emission lines (OB97). Motivated by these similarities, we observed the counterpart of 4U 1543-47 and discovered that the second hypothesis of Chevalier (1989) is the correct one—the A star is in fact the mass donor, although in view of GRO J1655-40 with its F-star secondary, the A star is perhaps not an “unusual” mass donor. We describe below our observations and

reductions, data analysis, and conclusions.

2. Observations and Reductions

Images of 4U 1543-47 were obtained 1997 June 28–July 3 with the CTIO 1.5 m telescope, the Tek 1024 \times 1024 #2 CCD at the $f/7.5$ focal position, and standard B , V , and I filters. The nights were generally clear during the time 4U 1543-47 was visible, and the seeing ranged from $1''.5$ to $2''.2$. Standard IRAF tasks were used to process the images to remove the electronic bias and to perform the flat-field corrections. Observations of several standard star fields from Landolt (1992) taken June 28 and June 29 were used to calibrate the photometry to the standard system. The calibrations from the two nights agreed to within 0.02 magnitudes.

Spectra of 4U 1543-47 were taken 1997 July 1-4 at the V. M. Blanco 4 m telescope at CTIO using the R-C spectrograph and the Blue Air Schmidt camera + Loral 3072 \times 1024 CCD. To reduce the readout noise, the CCD was binned on chip by 2 in the spatial direction. The KPGL #3 grating (527 ℓ /mm, first order) and the blue collimator were used on the night of July 1. The resulting “blue spectra” cover the wavelength range 3466-7162 \AA in 1.2 \AA pixels; the spectral resolution is about 3.6 \AA FWHM. The G420 grating (600 ℓ /mm, first order) and the red collimator were used the nights of July 2-4 to obtain “red spectra” that cover 5820-9130 \AA with 1.08 \AA pixels and have a spectral resolution of about 3.3 \AA FWHM. The seeing was typically $1''.0$ to $1''.5$, although on some occasions it reached $2''.0$. The nights of July 1-3 were photometric during the observations of 4U 1543-47. However on July 4 there was 1 to 2 magnitudes of extinction due to clouds. The slit width was fixed at $1''.5$ for all observations, and the slit angle was rotated to match the parallactic angle (Filippenko 1982) for all of the July 1-3 observations. The slit angle on July 4 was set to 90° (east-west) for the bright comparison stars and 75° for 4U 1543-47. Directly after the telescope was moved or the spectrograph was rotated, a He-Ne-Ar lamp was observed. During extended observations of 4U 1543-47, the lamp was observed every hour. The dispersion solutions are accurate to better than 0.1 \AA , and the maximum spectrograph flexure that occurred during an entire night was less than 2 pixels. We obtained a total 41 of spectra of 4U 1543-47 over the 4 nights with exposure times of 900-1200 seconds. We also obtained 28 spectra of 12 differ-

ent A-type comparison stars, 13 spectra of 12 IAU radial velocity standard stars, 10 spectra of 4 different flux standard stars, and 9 spectra of 4 different O stars (used to help locate telluric water vapor bands in the red spectra; Wade & Horne 1988). Finally, George Jacoby kindly took two spectra of 4U 1543-47, the spectrum of an A0V comparison star, and the spectrum of a flux standard using the Blanco 4 meter telescope in photometric conditions on the night of 1997 June 29. He used the spectrograph, camera, and detector mentioned above, and the #181 grating (316ℓ/mm, first order). These spectra cover 4700 to 10,028 Å in 2.0 Å pixels, giving a spectral resolution of about 6 Å FWHM.

IRAF tasks were used to remove the electronic bias and to perform the flat-field corrections of the 2-D spectra. Then optimal extractions (Horne 1986) of the spectra were done with the programs in the CTIOSLIT package within IRAF. The profile of 4U 1543-47 was well resolved from the profiles of its near neighbors (see below), and the quality of our spectra is generally quite high. The signal-to-noise (S/N) ratios of our blue 4U 1543-47 spectra are 30 to 40 per pixel near 5000 Å, while the S/N ratios of the red spectra are 40 to 60 per pixel near 7000 Å; however a few of the most weakly exposed spectra from July 4 have S/N ratios as low as 20 per pixel. The S/N ratios for the bright comparison A-type stars are in excess of 150 per pixel.

3. Period Determination

3.1. Spectroscopic Period

The radial velocities were determined from the spectra by cross-correlating an “object” spectrum with a “template” spectrum as described in Tonry & Davis (1979). The calculations were done using FXCOR within IRAF. For the blue spectra, the cross-correlation (CC) functions were computed simultaneously over the wavelength intervals 3750-4455, 4525-5750, and 6310-6715 Å, which includes all of the Balmer lines up to H12, and excludes some strong interstellar lines such as the NaI D lines. The CC functions for the red spectra were computed over the wavelength intervals 6310-6840, 7000-7100, 7350-7550, 7700-8050, and 8370-8700 Å. We used observations of the O stars at several different airmasses to locate the strongest telluric water vapor lines in the red spectra (Wade & Horne 1988), and the CC region was carefully picked to avoid the telluric bands. The

strongest A-star lines in this CC region are Hα and lines 13 to 17 of the Paschen series.

The radial velocities of 4U 1543-47 were measured using the A0V star HD 130095 as the template. This comparison star was observed by us six times over the four nights and was also observed by Jacoby the night of June 29. We adopted the first observation from July 1 as the template for the blue spectra and the first observation from July 2 as the template for the red spectra. For every object spectrum the CC was quite strong with a peak height ranging from 0.55 to 0.80. The velocity corresponding to the maximum of the CC functions was determined by making a parabolic fit to the seven pixels centered on the peak. Typical values for the “r” parameter (Tonry & Davis 1979) ranged from 15 to 25.

The spectroscopic period was found by fitting a three-parameter sinusoid to the resulting 43 velocities over a range of trial periods. We then looked for the trial period P which resulted in the lowest value of χ_ν^2 . The three free parameters are the epoch of maximum velocity T_0 , the semi-amplitude K_2 , and the systemic velocity γ . Figure 1 shows how χ_ν^2 varies as a function of the trial period. The best sinusoid fit to the radial velocities has a period of $P = 1.123$ days, where $\chi_\nu^2 = 0.448$. The one day alias period ($P = 0.529$ days) is clearly ruled out, since $\chi_\nu^2 = 5.75$ at that period. The errors on the radial velocities were scaled to give $\chi_\nu^2 = 1$, and the uncertainties on the fitted parameters were computed using the scaled errors. The period of $P = 1.123 \pm 0.008$ days and the semi-amplitude of $K_2 = 124 \pm 4$ km s⁻¹ combine to give a mass function of $f(M) = 0.22 \pm 0.02 M_\odot$. Table 1 gives the orbital parameters and Figure 2 shows the velocities and the best-fitting sinusoid.

One must be cautious when dealing with periods near one day. Flexure in the spectrograph could in principle produce a spurious signal if one observes a source at the same hour angles each night. However, an examination of the residuals (the data *minus* the model fit) shown in Figure 2 shows that there are no systematic trends evident. Furthermore, our period search excludes values near 1.0 days, as shown in the upper panel of Figure 1. Based on our past experience with this spectrograph and the reliable results we have obtained (McClintock & Remillard 1990; Remillard, McClintock, & Bailyn 1992; Bailyn et al. 1995b; Remillard et al. 1996; Orosz et al. 1996), we are confident that $P = 1.123 \pm 0.008$ days is the true orbital period of 4U 1543-47.

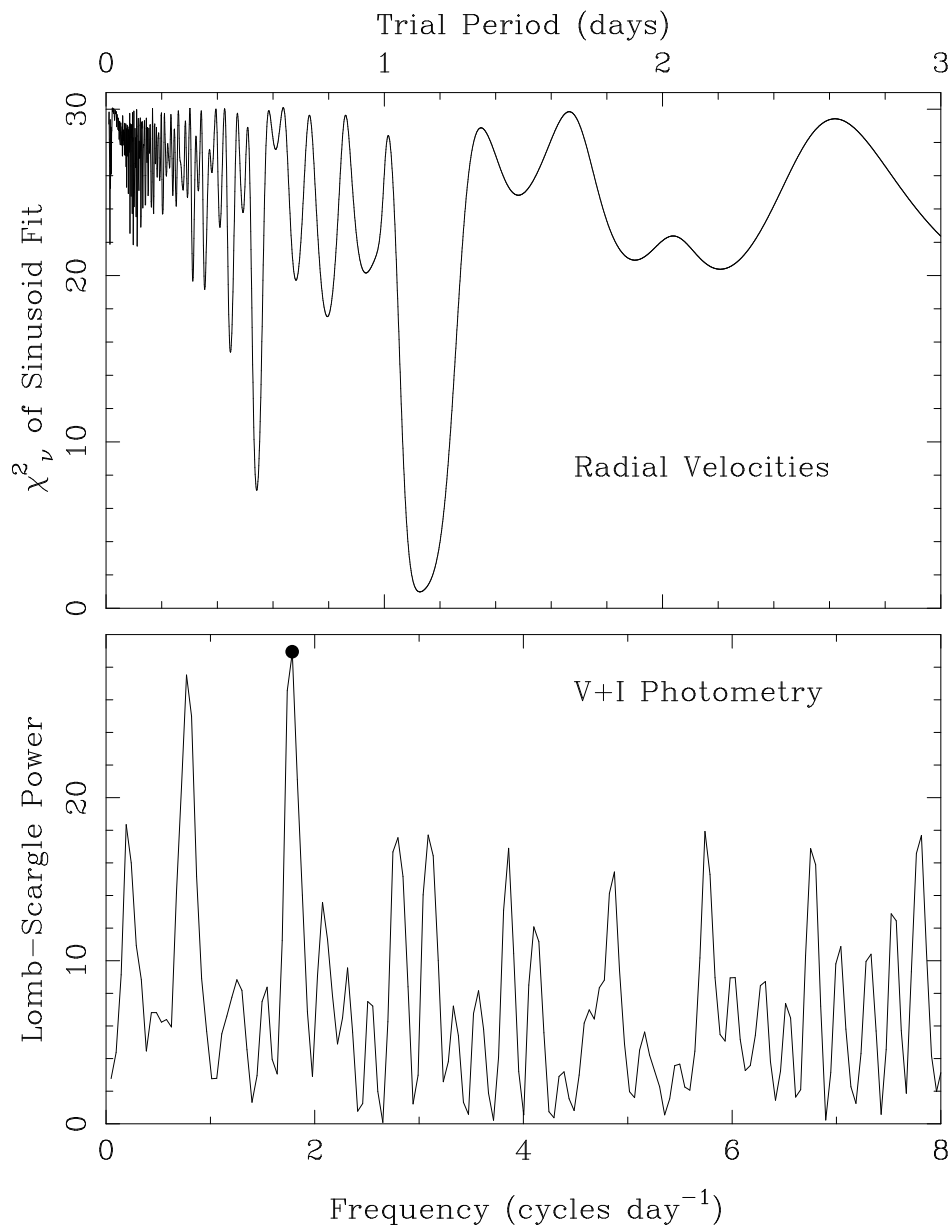


Fig. 1.— Top: The value of χ^2_ν of a sinusoid fit to the 43 radial velocities as a function of the trial period. The best fitting sinusoid has a period of $P = 1.123$ days. Bottom: A Lomb-Scargle periodogram for the combined $V + I$ light curve. The highest peak (marked with a filled circle) has a frequency of 1.784 cycles day^{-1} , corresponding to a period of $P = 0.5605$ days $= P_{\text{spect}}/2$. The “false-alarm probability” for this peak is 1.3×10^{-10} .

TABLE 1
PARAMETERS FOR 4U 1543-47

parameter	value
Spectroscopic period P (days)	1.123 ± 0.008
T_0 (HJD 2,450,000+)	629.6329 ± 0.0083
K_2 velocity (km s^{-1})	124 ± 4
γ velocity (km s^{-1})	-87 ± 3
$f(M)$ (M_\odot)	0.22 ± 0.02

3.2. Photometric Period

It is relatively difficult to obtain precise photometry of 4U 1543-47 since there is a star $7''.25$ to the southeast that is ≈ 4.5 mag brighter in V than the counterpart. In addition, there is a faint red star $2''.5$ to the northeast of the counterpart which is ≈ 4 magnitudes fainter in V . Simple aperture photometry would be inadequate, so we used the programs DAOPHOT IIe, ALLSTAR and DAOMASTER (Stetson 1987; Stetson, Davis, & Crabtree 1991; Stetson 1992a,b) to compute the photometric time series of 4U 1543-47 and the ≈ 1000 other stars in the field. DAOPHOT was used to construct an empirical point spread function (PSF) for each frame from fits to relatively isolated bright stars. Then the PSFs were used to deblend close stars, thereby making it possible to do accurate photometry in the crowded field. The exposure times were adjusted so that only a few pixels of the bright neighbor star were saturated, while leaving the image of 4U 1543-47 relatively well-exposed. DAOPHOT and ALLSTAR were then used to remove the wings of the bright star’s profile. The resultant S/N ratios in the images of 4U 1543-47 were still adequate for precise photometry. The DAOMASTER program assembles the photometric time series from the individual photometry files by effectively using as comparison stars all of the stable stars that are common to all of the images. In this way the derived light curves are not sensitive to the fluctuations of a few comparison stars.

Both the V and I light curves of 4U 1543-47 show statistically significant variations. For example, the standard deviation (from a constant mean value) of the V -band light curve of 4U 1543-47 is 0.038, compared to 0.005 to 0.01 for the ≈ 30 field comparison

stars with brightnesses similar to that of 4U 1543-47. The amplitude of the I light curve is about 0.015 magnitudes less than the amplitude of the V light curve. We combined the V and I photometry after subtracting the mean from each set and searched for periodicities by computing the Lomb-Scargle periodogram (Figure 1) using an implementation due to Press et al. (1992). The highest peak in the periodogram for the combined $V + I$ band data has a frequency of 1.784 cycles per day, corresponding to a period of 0.5605 days. This is one-half of the spectroscopic period (to within the error of P_{spect}), as expected for an ellipsoidal light curve with two maxima and two minima per orbital cycle. This main peak is about 60% taller than all of the other peaks (except for the one day alias peak at 0.784 cycles per day) and has a “false-alarm probability” of 1.3×10^{-10} , where a small value of this probability indicates that significant periodic signal is present (Press et al. 1992).

We expect to see an ellipsoidal light curve with a period equal to the spectroscopic period because the secondary is Roche lobe-filling (i.e. there are X-ray outbursts caused by accretion onto the compact object) and is the dominate source of optical light in the system (Section 4). In several other black hole binaries the *quiescent* photometric period (of the ellipsoidal modulation) has been shown to be the same as the spectroscopic period derived from the secondary star’s absorption line radial velocity curve: A0620-00 (McClintock & Remillard 1986; Orosz et al. 1994), GRS 1124-683/XN Mus91 (Orosz et al. 1996; Casares et al. 1997), H1705-250/XN Oph77 (Remillard et al. 1996; Filippenko et al. 1997), GRO J1655-40 (Orosz & Bailyn 1997; van der Hooft et al. 1997), and GRO J0422+32 (Orosz 1996; Filippenko, Matheson, & Ho 1995). Based on these considerations and given the

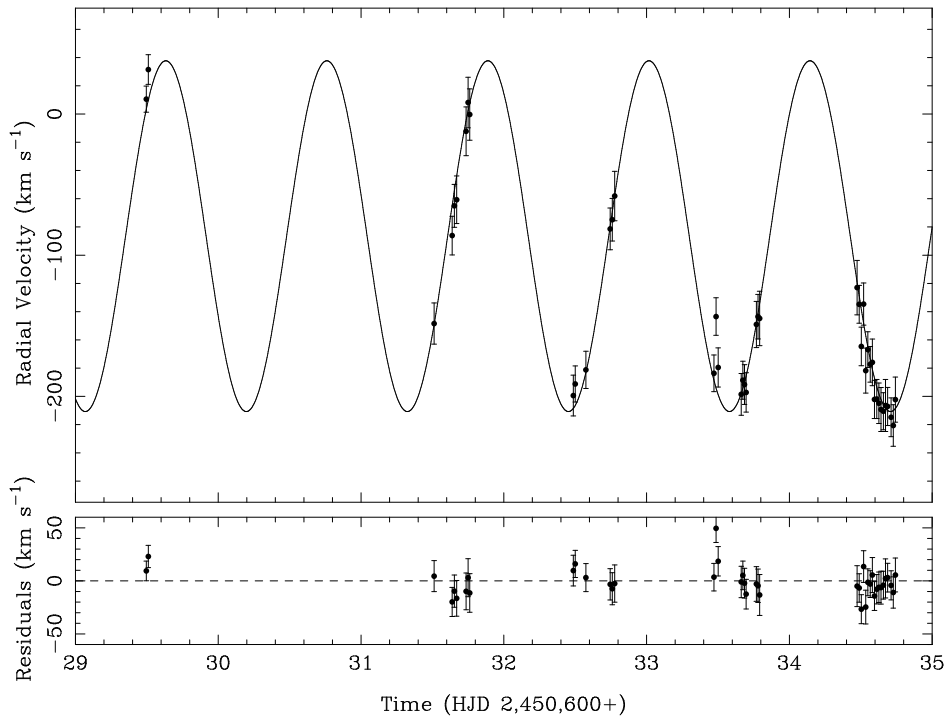


Fig. 2.— Top: The radial velocities of 4U 1543-47 and the best-fitting sinusoid (solid line). The errors on the velocities have been scaled so that reduced chi-square of the sinusoid fit is 1.0. Bottom: The residuals in the sense of the data *minus* the model fit.

fact that the highest peak in the periodogram has a period of $P_{\text{spect}}/2$, we are justified in asserting that $P_{\text{photo}} = P_{\text{spect}}$ for 4U 1543-47.

The traditional definition of the photometric phase is $T_0(\text{photo}) = T_0(\text{spect}) + 0.75P$ (i.e. $T_0(\text{photo})$ corresponds to the time of the closest approach of the A-star). We estimated $T_0(\text{photo})$ in two different ways. A sinusoid with a period of 0.5605 days fit to the V band data gives $T_0(\text{photo}) = \text{HJD } 2,450,629.380 \pm 0.013$ (although in this case there is a half cycle ambiguity). A fit using an ellipsoidal model (see Section 5 below) gives $T_0(\text{photo}) = \text{HJD } 2,450,629.362 \pm 0.012$ (there is no half cycle ambiguity in this case). We adopt a value that is the average of the two: $T_0(\text{photo}) = \text{HJD } 2,450,629.37 \pm 0.01$. The spectroscopic phase of $T_0(\text{photo})$ is 0.733 ± 0.013 , consistent with the expected value of 0.75. This agreement between the photometric and spectroscopic phases has an a priori probability of ≈ 0.1 , which further increases the significance of the peak at 0.5605 days.

The V and I light curves of 4U 1543-47 (corrected to the standard magnitude scales) are shown in Figure

3 folded on the photometric phase. The right panels in Figure 3 show the light curves binned into 12 phase bins (where a few of the bins are empty). Although the light curves are somewhat noisy, they resemble an ellipsoidal light curve because they have maxima at phases consistent with 0.25 and 0.75 and minima at phases consistent with 0.0 and 0.5. The amplitudes of the light curves are small, roughly 0.08 magnitudes in V and 0.07 magnitudes in I . The ellipsoidal models shown with the binned light curves are discussed below in Section 5. Note that the existence of ellipsoidal variations implies that the A star is the mass donor and not the outer star of a triple system.

4. Spectral Classification and Reddening

Figure 4 shows the blue “restframe” spectrum of 4U 1543-47 and the spectra of several A-type comparison stars. (The restframe spectrum is a sum of the individual spectra, which have been corrected to zero velocity). The spectrum of 4U 1543-47 was dereddened using $E(B - V) = 0.5$ (see below). The Ca II K line at 3933 \AA is a strong temperature indicator in

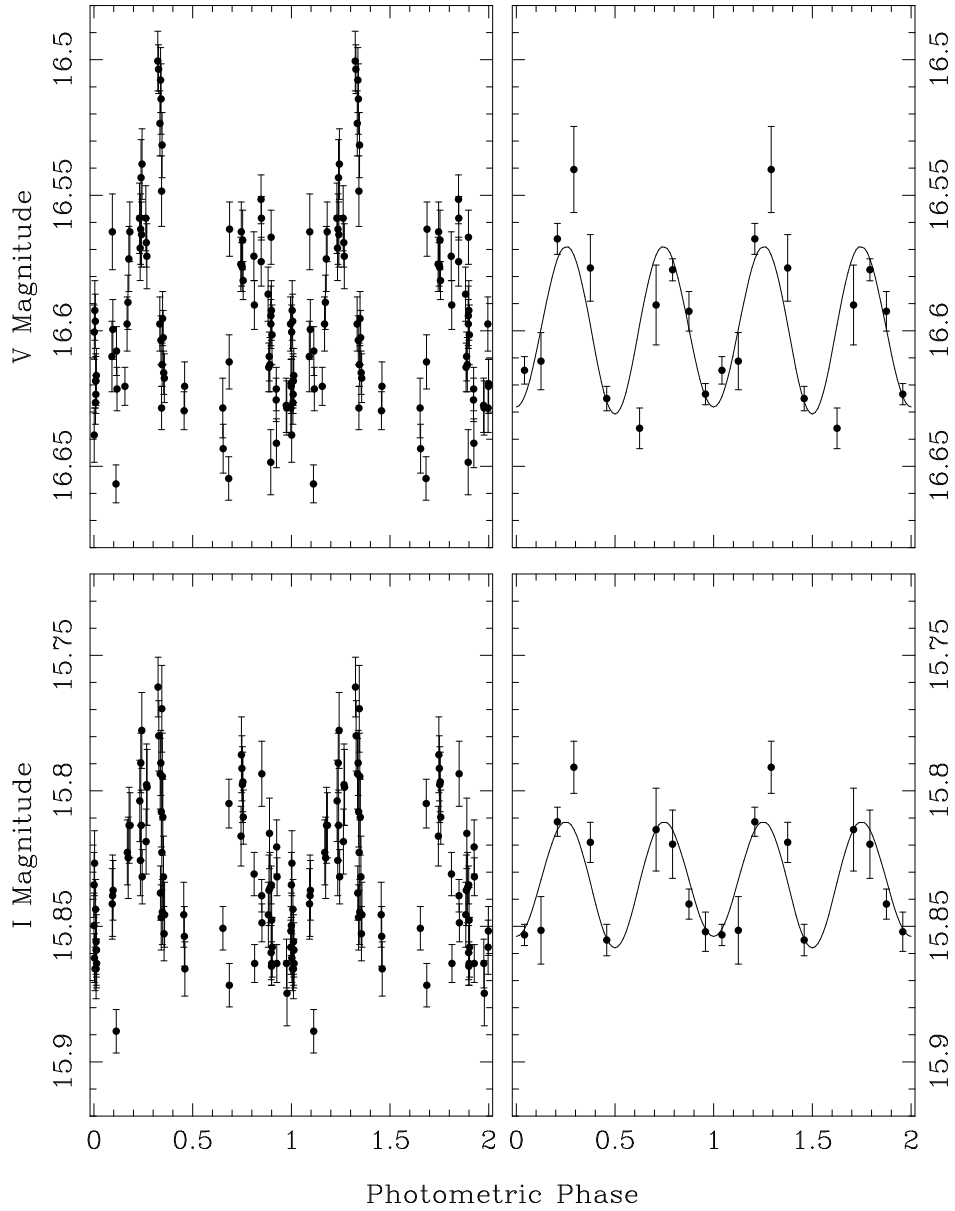


Fig. 3.— The left panels show the V and I light curves of 4U 1543-47 folded on the photometric phase, where $T_0(\text{photo}) = T_0(\text{spect}) + 0.75P$. The right panels show the folded light curves binned into 12 phase bins. Note that a few of the bins are empty. The curves shown are an ellipsoidal model with an inclination of 31° and a mass ratio of 2.

A stars, and its equivalent width of 2.1 \AA gives a spectral type of A2-A3 (Jaschek & Jaschek 1987). Some of the K line could be due to interstellar absorption, in which case the spectral type would be slightly earlier. In principle, the widths of the Balmer lines can be used as a luminosity indicator in A stars (Jaschek & Jaschek 1987), but the difference in widths between dwarfs and subgiants is too small for us to measure. We will adopt a spectral type of A2V, the same type determined by Chevalier (1989).

Our broad spectral coverage affords us a good opportunity to make an independent estimate of the reddening. The precision of our absolute flux calibration was compromised by the use of a narrow slit; however, the relative spectrophotometry should be much better since we rotated the spectrograph slit to match the parallactic angle, thereby minimizing the effects of differential atmospheric refraction (Filippenko 1982). Indeed, the flux values of the restframe spectra from June 29 and July 1 agreed to better than 1% between 4700 and 6560 \AA after each spectrum was normalized to unity at 5000 \AA (there was about a 5% difference between the two spectra between the $H\alpha$ line and the telluric A band). We averaged the two normalized restframe spectra to create a continuous spectrum from 3600 to 9100 \AA .

We used synthetic spectra generated from Kurucz models with solar metallicity to decompose the spectrum of 4U 1543-47 into its stellar and disk components. The observed A-star comparisons made unsuitable templates because of the broad temperature range and the large line broadening due to rapid rotation. The decomposition technique we used has been discussed elsewhere (Marsh, Robinson, & Wood, 1994; Casares & Charles 1994; OB97). Basically a normalized template spectrum is scaled by a factor w , subtracted from the normalized restframe spectrum, and the scatter in the difference spectrum is measured by computing the rms (per 1.2 \AA bin) from a polynomial fit (with interstellar and telluric lines masked out of the fit). The process is repeated until the “smoothest” difference spectrum is found (corresponding to the lowest overall rms from the polynomial fit). The smoothest difference spectrum is taken to be the spectrum of the disk. The relative contributions of the star and disk to the total system flux can be measured by looking at the relative levels of the restframe spectrum and the scaled template spectrum. In our case we first dereddened the restframe spectrum by various amounts and used syn-

thetic template spectra characterized by several different effective temperatures (T_{eff}) and surface gravities ($\log g$). We then looked for the combination of $E(B - V)$, T_{eff} , and $\log g$ that gave the smoothest overall difference spectrum. The best combinations were for $8500 < T_{\text{eff}} < 9500 \text{ K}$, $3.5 < \log g < 4.0$, and $0.45 < E(B - V) < 0.55$. Figure 5 shows an example of a decomposition where the restframe spectrum was dereddened using $E(B - V) = 0.5$ and where the synthetic spectrum has $T_{\text{eff}} = 9500$ and $\log g = 4.0$. The temperature range of $8500 < T_{\text{eff}} < 9500 \text{ K}$ corresponds roughly to a spectral type range of A1 to A3 (Gray 1992).

For comparison, our derived range of values for the color excess ($0.45 < E(B - V) < 0.55$) is slightly lower than the range derived from X-ray observations. The hydrogen column density N_H estimated from X-ray spectra ranges from $3.1 \times 10^{21} \text{ cm}^{-2}$ (Greiner et al. 1994) to $(4.26 \pm 0.15) \times 10^{21} \text{ cm}^{-2}$ (van der Woerd et al. 1989). The implied values of the color excess $E(B - V)$ range from 0.56 to 0.77 assuming $A_V = N_H/1.79 \times 10^{21}$ (Predehl & Schmitt 1995) and $E(B - V) = A_V/3.1$. Note that there may be a significant contribution to N_H due to X-ray absorption in 4U 1543-47 itself, in which case the derived values of N_H and $E(B - V)$ would be inflated.

The disk spectrum shown in Figure 5 is approximately flat across the entire range, although the relatively poor S/N at the blue end makes it difficult to assess the precise spectral shape there. With the exception of $H\alpha$, the disk spectrum is free of hydrogen lines in absorption, and is also devoid of emission lines. The accretion disk contributes roughly 10% of the flux in B , 21% in V , 32% in R , and 39% in I (the uncertainties in these values are $\lesssim 5\%$). Although the disk spectrum will be used as input to the ellipsoidal models discussed in Section 5, we will not discuss the disk spectrum further. A thorough discussion of the relative faintness of the disk, the lack of emission lines, and the overall spectral shape is beyond the scope of this paper.

5. Inclination Constraints

The amplitude of an ellipsoidal light curve depends strongly on the inclination of the binary orbit (Avni 1978). In practice, however, one must carefully assess the strength of extra sources of light, such as light from the disk. The small amplitudes of the light curves for 4U 1543-47 imply a small inclination (the

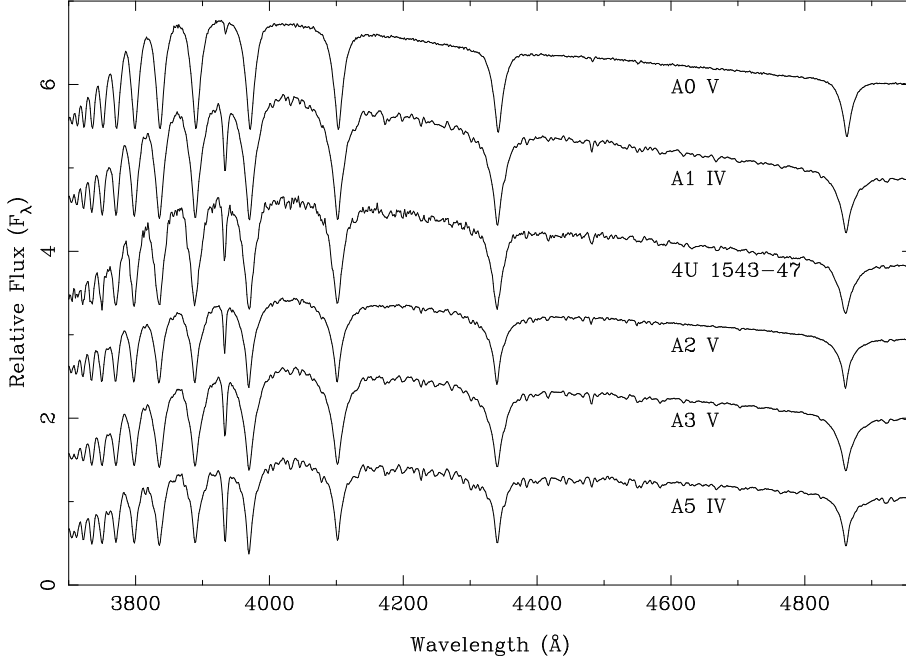


Fig. 4.— The dereddened blue restframe spectrum of 4U 1543-47 is shown along with the spectra of several A stars. All of the flux-calibrated spectra have been normalized to unity at 5000 Å and offsets have been applied for clarity.

disk is relatively faint and does not substantially reduce the amplitude of the observed light curves). We modeled the light curves using the modified version of the Avni (1978) code described in OB97 (also see Orosz & Bailyn 1997b). We assume the secondary star is in synchronous rotation and completely fills its Roche lobe. The effective temperature of the secondary was taken to be 9000K, and the limb darkening coefficients for a $\log g = 4$ atmosphere were taken from Wade & Rucinski (1985). The A-star has a radiative envelope, so the gravity-darkening exponent was set to 0.25 (see OB97). For 4U 1543-47, which is a non-eclipsing system, we used the empirically determined disk spectrum (Figure 5) as input to the modified Avni code. The continuum fit of the disk spectrum $D(\lambda)$ was divided by the continuum fit of the scaled stellar spectrum $S(\lambda)$, producing the “ratio spectrum” $R(\lambda)$. The code then determines the model disk spectrum for all phases by multiplying $R(\lambda)$ by the model star’s spectrum at phase 0.0. The model disk spectrum and the model star spectrum at each phase are summed and integrated with the filter response functions to produce the model flux in the five filters. This method of computing fluxes at several different wavelengths and then integrating with the filter response functions to get the final *UBVRI*

fluxes is much more accurate than simply computing the flux at the “effective” wavelength of each filter because the effective wavelength of the filter bandpasses depends on the shape of the input spectrum.

X-ray heating of the secondary star can alter the shape of the observed light curve when $L_x \gtrsim L_{\text{opt}}$ (e.g. Avni 1978). 4U 1543-47 was observed in the quiescent state 1996 February with the SIS detector on the *Advanced Spacecraft for Cosmology Astrophysics* (ASCA). We reanalyzed the publicly available data and found that the source was not detected after a 20.4 ksec observation, indicating an X-ray flux limit (0.5 - 10 keV) of $F_x \lesssim 2 \times 10^{-13}$ ergs $\text{s}^{-1} \text{cm}^{-2}$ ($\approx 5\sigma$), assuming a power law spectrum with an index of 2 and a hydrogen column density of $N_H = 3.5 \times 10^{21} \text{cm}^{-2}$. The corresponding X-ray luminosity limit is $L_x \lesssim 3.83 \times 10^{32} (d/4 \text{kpc})^2$ ergs s^{-1} , a typical value for a quiescent X-ray transient (Tanaka & Shibasaki 1996). We therefore neglect X-ray heating since the quiescent X-ray luminosity of the system is a very small fraction of the bolometric luminosity of the A-star secondary: $L_{\text{bol}} \gtrsim 95L_x$ for a distance of 9 kpc (Section 6.2).

Once the disk light is accounted for, the two remaining free parameters for the ellipsoidal model are

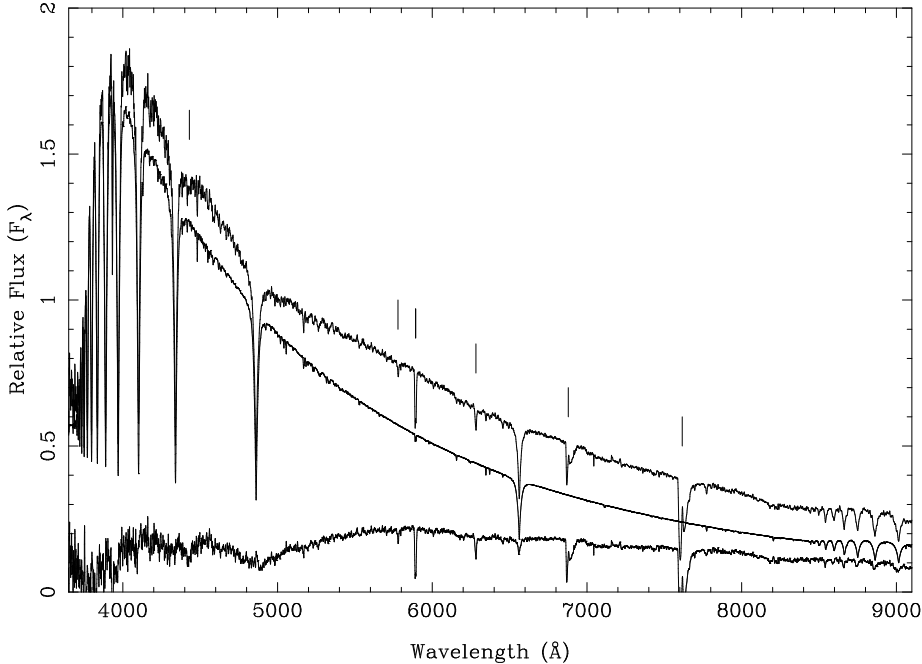


Fig. 5.— The normalized dereddened restframe spectrum of 4U 1543-47 made by averaging the spectra from 1997 June 29 and July 1 is shown on the top. The spectrum in the middle is a Kurucz model spectrum with $T_{\text{eff}} = 9500$ K and $\log g = 4.0$ scaled by 0.9. The difference spectrum is shown at the bottom. Strong interstellar and telluric lines are indicated with the vertical bars.

the inclination i and the mass ratio $Q \equiv M_1/M_2$, where M_1 is the mass of the compact primary and M_2 is the mass of the A-star secondary. Note that the individual component masses themselves are not important—the relative shapes of the Roche lobes depend only on the mass *ratio*. The binned V and I light curves were fit simultaneously, producing the χ^2 contours in the Q vs. i plane shown in Figure 6. The inclination is tightly constrained between 24° and 36° (the formal 3σ limits for $Q > 1$ corresponding to the $\chi^2 = \chi_{\text{min}}^2 + 9 = 66$ contours), while the mass ratio is basically unconstrained (i.e. the χ^2 contours are nearly parallel to the y -axis). We argue that the A-star is on the main sequence (see Section 6.1 below), which implies mass ratios near ≈ 2 . For mass ratios near 2, the $\chi^2 = 66$ contours enclose an inclination range of $27 \leq i \leq 36^\circ$. However, since we cannot immediately rule out the larger mass ratios, we adopt the wider range of inclinations: $24 \leq i \leq 36^\circ$.

The model light curves for $i = 31^\circ$ and $Q = 2$ are shown as the solid lines in Figure 3. Except for some excess light near phase 0.25, the $i = 31^\circ$ models fit the light curves reasonably well. Excess light has been seen in the light curves of Nova Muscae 1991 (Orosz et al. 1996) and GRO J0422+32 (Casares et al.

1995; Orosz 1996). Orosz et al. (1996) argued that the asymmetry in the light curves of Nova Muscae 1991 was due to extra phase-modulated light from the accretion disk and that a model fit to the smaller maximum and the two minima should be more trustworthy. If the asymmetry of the 4U 1543-47 light curves is also due to phase-modulated light from the disk, then the model fits to the 4U 1543-47 light curves shown in Figure 3 should be fairly reliable. In any event, the presence of the excess light near phase 0.25 and the large χ^2/DOF (≈ 2.9 at the minimum) does indicate unaccounted for systematic effects, so the inclination limits quoted above should be treated with caution. Light curves with better phase coverage and higher statistical precision will be needed before definitive inclination limits can be established.

We can derive a lower limit on the inclination by fitting a model that has no disk contamination. A model with $i = 20^\circ$ and $Q = 10$ has an amplitude between phases 0.75 and 1.0 which is $\approx 15\%$ smaller than the amplitudes of the observed light curves in the same phase interval. Since the addition of disk light will act to reduce the amplitude of the observed light curve, we can adopt $i \geq 20^\circ$ as a reasonable lower limit on the inclination since the inclination of

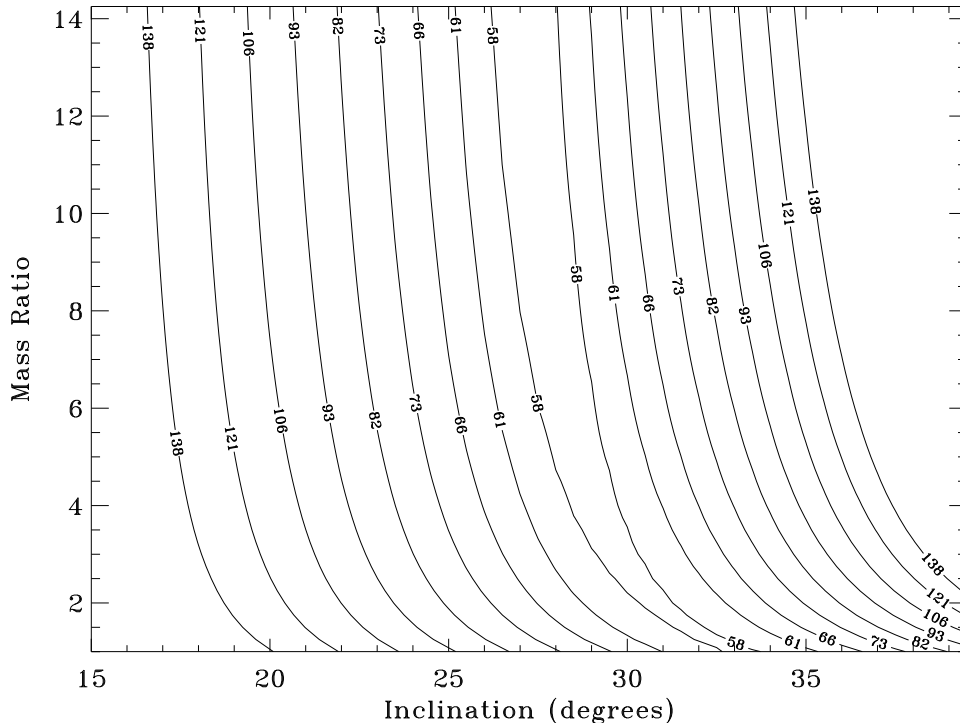


Fig. 6.— χ^2 contours for simultaneous ellipsoidal model fits to the V and I binned light curves. There are 11 points in the V light curve and 10 points in the I light curve. The minimum χ^2 value is 57.32. The contours levels are $\chi_{\min}^2 + 1$, $\chi_{\min}^2 + 4$, $\chi_{\min}^2 + 9$, etc. The formal 3σ inclination range is $24 \leq i \leq 36^\circ$ while the mass ratio is not well-constrained. A fit to the unbinned light curves produces a similar contour plot.

the model will need to increase in order to match the observations. Similarly, a model with $i = 40^\circ$, $Q = 2$, and a 21% disk fraction in V (i.e. the observed value) has an amplitude between phases 0.25 and 0.50 \approx 15% larger than the amplitudes of the observed light curves in the same phase interval. The difference in amplitudes is \approx 25% between phases 0.75 and 1.0. We will adopt $i \leq 40^\circ$ as an upper limit on the inclination. These extreme inclination limits correspond roughly to the $\chi^2 = \chi_{\min}^2 + 49 = 106$ contours shown in Figure 6.

6. Discussion

6.1. Constraints on the Component Masses

One can easily compute the mass of the compact primary M_1 when given the mass function $f(M)$, the inclination i , and the mass of the A-star secondary M_2 :

$$f(M) \equiv \frac{PK_2^3}{2\pi G} = \frac{M_1^3 \sin^3 i}{(M_1 + M_2)^2}. \quad (1)$$

Figure 7 shows plots of M_1 as a function of M_2 for $i = 20, 30$, and 40° (solid lines, left y -axis scale). We must now consider the possible values of the secondary star mass M_2 in order to derive useful limits on the mass of the compact primary.

It is clear from the spectra (Figure 4) and the models (Section 4) that the secondary star is an early A-star with $T_{\text{eff}} \approx 9000$ K. If the A-star is on the main sequence, then we would expect its mass to be near $\approx 2.2 M_\odot$ (Gray 1992). On the other hand, the secondary star could be a highly evolved star on the extended horizontal branch (EHB) where it would have a He burning core and a thin H envelope and a mass of $\approx 0.5 M_\odot$. Initially, one might expect that the main sequence star would have a rather different surface gravity than the EHB star, which would lead to rather different Balmer line profiles (e.g. Jaschek & Jaschek 1987). However, the following simple exercise shows that the surface gravity ($\log g$) of the secondary star varies by only a small amount over a wide range of masses M_2 . The mean density of the secondary star

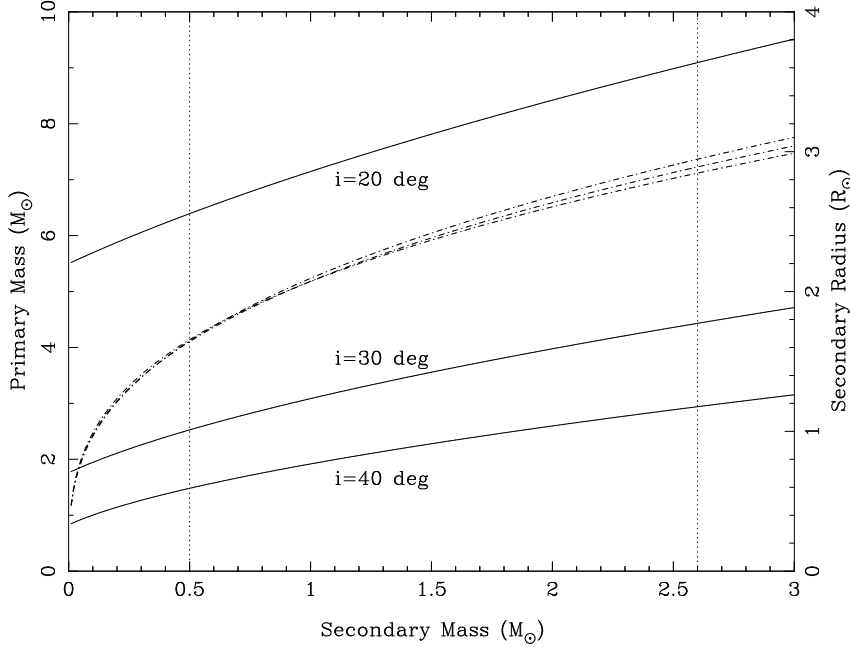


Fig. 7.— The mass of the primary M_1 (solid lines, left y -axis scale) and the radius of the secondary R_2 (dash-dotted lines, right y -axis scale) as a function of the secondary star mass M_2 for a mass function of $f(M) = 0.22 M_{\odot}$ and $i = 20, 30,$ and 40° . The vertical dotted lines indicate the extreme range of secondary star masses $0.5 \leq M_2 \leq 2.6 M_{\odot}$.

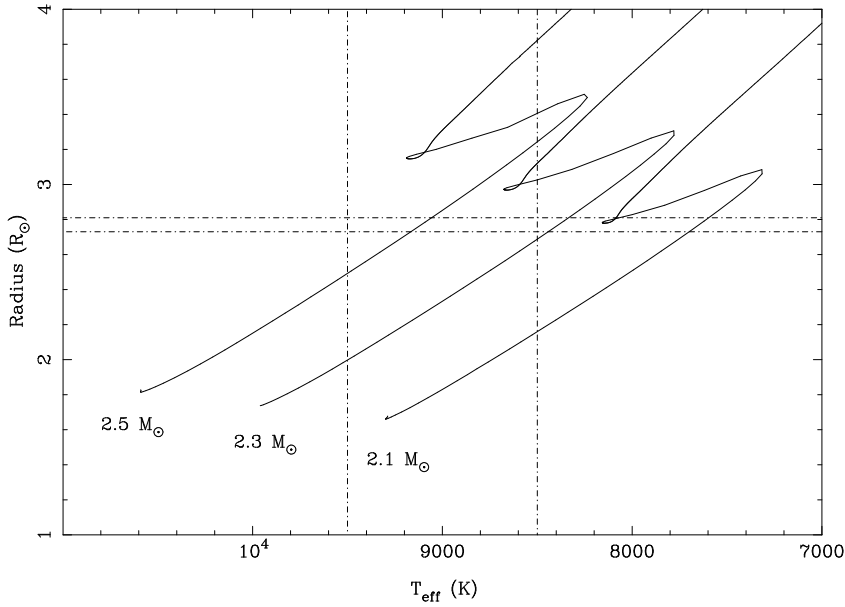


Fig. 8.— The radius of the model stars as a function of the effective temperature. The stars begin H burning at the lower left and move to larger radii and cooler temperatures as they age. Core H burning stops just beyond the tiny loops in the tracks. The vertical lines indicate the range of temperatures measured for the 4U 1543-47 secondary, and the horizontal lines correspond to the range of radii of a star with $2.1 \leq M_2 \leq 2.5 M_{\odot}$ (see Figure 7).

depends only on the orbital period to a very good approximation (Pringle 1985), i.e. $\rho_2 \approx \text{const}$. This implies $R_2 \propto M_2^{1/3}$ (Figure 7, dashed-dotted lines, right y -axis scale). Since $g \propto M_2/R_2^2$, $\log g \propto 1/3 \log M_2$. The difference in the $\log g$ values between the main sequence star and the EHB star would be less than 0.25, which is too small for us to measure using our current spectra.

A strong indication that the secondary star probably is on the main sequence comes from an examination of stellar models. We computed the evolutionary tracks of a $2.1 M_\odot$ star, a $2.3 M_\odot$ star, and a $2.5 M_\odot$ star using the Yale Stellar Evolution Code (Guenther et al. 1992) with updated opacities (Iglesias & Rogers 1996). We assumed solar metallicity, a hydrogen abundance of 71%, and a mixing length coefficient of 1.7, all typical values for population I stars. The radius of these model stars as a function of the effective temperature is shown in Figure 8. The vertical lines indicate the likely range of the temperature of the 4U 1543-47 secondary star, and the horizontal lines indicate the range of radii of the secondary star when $2.1 \leq M_2 \leq 2.5 M_\odot$ (Figure 7). The $2.5 M_\odot$ star appears on the zero-age main sequence (ZAMS) hotter than the secondary star in 4U 1543-47. However, the $2.5 M_\odot$ star will expand and cool *while on the main sequence* until it attains a temperature of ≈ 9000 K (the observed temperature of the secondary star) and a radius of $\approx 2.8 R_\odot$, which is precisely the radius the secondary star in 4U 1543-47 would have if $M_2 = 2.5 M_\odot$ (Figure 7). In fact, stars with $2.3 \lesssim M_2 \lesssim 2.6 M_\odot$ will pass through the thin box in the center of Figure 8 during their main sequence lifetimes (≈ 393 Myr past the ZAMS in the case of the $2.5 M_\odot$ star). One should note that the evolutionary tracks shown in Figure 8 are for *single* stars. The secondary star in 4U 1543-47 has been losing mass, and this is not accounted for in the evolution models. However, Kolb et al. (1997) show that in the case of GRO J1655-40 (whose secondary has a mass similar to that of 4U 1543-47 but is roughly twice the age (OB97)), the proper binary evolution models which account for the mass loss give similar results as the single star evolutionary models. Therefore the single star models applied to 4U 1543-47 should also be a good approximation since it is a younger system.

We conclude the secondary star is probably on the main sequence based on the fact that the mean density of the secondary is consistent with the mean density of a main sequence star with the same spectral

type. This conclusion does not depend on any assumed value of the inclination since the computed radius of the secondary in 4U 1543-47 is a very weak function of the inclination. We adopt a mass range of $2.3 \leq M_2 \leq 2.6 M_\odot$ for the A-star secondary. Using these main sequence values for the secondary star's mass, the best fits for the 3σ inclination range ($24 \leq i \leq 36^\circ$) and 3σ mass function range ($0.16 \leq f(M) \leq 0.28 M_\odot$) imply a primary mass in the range $2.7 \leq M_1 \leq 7.5 M_\odot$.

We can derive an extreme lower limit on the primary mass M_1 by adopting the following extreme values of the parameters: $M_2 = 0.5 M_\odot$ and $i = 40^\circ$. In addition, we adopt $f(M) = 0.16 M_\odot$, which is the 3σ lower limit on the mass function, and conclude: $M_1 \geq 1.2 M_\odot$. Thus the primary mass is at least $1.2 M_\odot$, and in fact is probably in excess of $2.7 M_\odot$ (i.e. the lower end of the range given above for main sequence secondary). The widely adopted maximum mass of a stable neutron star is $M_{\text{max}} \approx 3 M_\odot$. We therefore conclude that this compact object is likely to be a black hole.

6.2. Constraints on the Distance and Peak X-ray Luminosity

We can easily compute the distance to the source once some basic assumptions are made. The distance d depends mainly on the secondary star mass M_2 and on the color excess $E(B - V)$; the dependence of d on the inclination i is very weak. The strong dependence of d on M_2 comes about because the orbital period fixes the mean density of the Roche lobe-filling secondary star. The secondary star mass M_2 can then of course be combined with the density to get the effective radius R_2 . For a main sequence secondary we compute $R_2 = 2.84 \pm 0.11 R_\odot$ for $20 \leq i \leq 40^\circ$ and $2.3 \leq M_2 \leq 2.6 M_\odot$. For the low mass end ($M_2 = 0.5 M_\odot$) we compute $R_2 = 1.65 \pm 0.07 R_\odot$. Once the radius is known, we can take the well-determined temperature of the secondary ($T_{\text{eff}} = 9000 \pm 500$ K) and apply the Stefan-Boltzmann relation to get the luminosity⁴. The distance modulus can be found after light from the accretion disk ($21 \pm 5\%$ of the total light

⁴Note that standard tables relating spectral type to luminosity such as the one given in Gray (1992) often give the absolute magnitude of the star *when it is on the ZAMS*. However, as shown in Figure 8, main sequence stars with similar temperatures can have a large range of radii, resulting in a large range of luminosities. Thus our method of finding the intrinsic luminosity of the secondary is more precise.

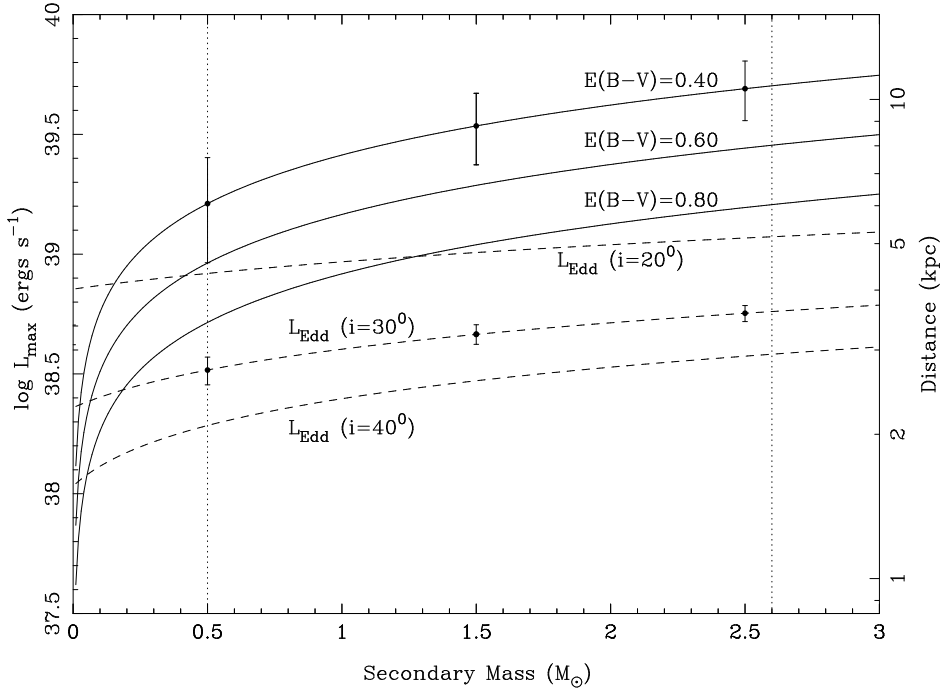


Fig. 9.— The solid lines show the peak X-ray luminosity during the 1983 outburst L_{\max} as a function of the secondary star mass M_2 (left y -axis scale) for three values of $E(B - V)$. The right y -axis scale shows the corresponding distances. The dashed lines show the Eddington luminosity as a function of M_2 for $i = 20, 30$, and 40° . The points on the upper solid line show the statistical error on L_{\max} due to the errors on T_{eff} , R_2 , and the disk fraction when $E(B - V) = 0.40$. The points on the middle dashed line show the statistical error on L_{Edd} due to the errors on the period P and the mass function $f(M)$ when $i = 30^\circ$.

in V) is accounted for and the reddening correction is made. There are two measurements of $E(B - V)$ we will consider: $E(B - V) = 0.50 \pm 0.05$ derived by us and $E(B - V) = 0.66 \pm 0.10$ found from the range of N_H determinations discussed above. Table 2 gives the 4 distance determinations made from the 2 values of R_2 and the 2 values of $E(B - V)$. Our preferred value is $d = 9.1 \pm 1.1$ kpc (this assumes our spectroscopically determined value of $E(B - V)$ and a main sequence secondary), which is more than a factor of two larger than the commonly assumed distance of 4 kpc (e.g. Chevalier 1989). The peak X-ray luminosity during the 1983 outburst is also given, where $L_{\max} = 7.08 \times 10^{38} (d/4 \text{ kpc})^2 \text{ ergs s}^{-1}$ (conservatively estimated assuming a thermal bremsstrahlung spectrum; Kitamoto et al. 1984). The quoted errors on d were computed assuming the given errors on the input parameters are 1σ Gaussian errors.

To better visualize how the distance d (and hence

L_{\max}) depends on M_2 and $E(B - V)$, we show in Figure 9 plots of $\log L_{\max}$ vs. M_2 for several values of $E(B - V)$. We have assumed $T_{\text{eff}} = 9000$ K, $\bar{V} = 16.6$, and a disk fraction of 21% in V . We also show the Eddington luminosity ($L_{\text{Edd}} = 1.3 \times 10^{38} (M/M_\odot) \text{ ergs s}^{-1}$) as a function of M_2 for $i = 20, 30$, and 40° (in contrast to L_{\max} , L_{Edd} does depend on i since L_{Edd} scales as the mass of the compact object). To give some idea of the uncertainties, we show the statistical error on L_{\max} due to the errors on T_{eff} , R_2 , and the disk fraction when $E(B - V) = 0.40$ for various values of M_2 . Likewise we show the statistical errors on L_{Edd} due to the errors on the period P and the mass function $f(M)$ when $i = 30^\circ$ for the same values of M_2 . For most of the values of M_2 , i , and $E(B - V)$, the derived maximum X-ray luminosity during the 1983 outburst exceeds the Eddington limit by an amount much larger than the errors. For example, for our preferred value of $d = 9.1$ kpc, $L_{\max} = 3.6 \times 10^{39} \text{ ergs s}^{-1}$. In this case the mass

TABLE 2
DISTANCE DETERMINATIONS FOR 4U 1543-47^a

Assumed Radius (R_{\odot})	$E(B - V)$	Secondary Luminosity (L_{\odot})	M_{bol}	Distance (kpc)	$\log L_{\text{max}}^{\text{b}}$ (ergs s ⁻¹)
$2.84 \pm 0.11^{\text{c}}$	0.50 ± 0.05	48 ± 11	0.51	9.1 ± 1.1	39.56 ± 0.11
2.84 ± 0.11	0.66 ± 0.10	48 ± 11	0.51	7.2 ± 1.0	39.36 ± 0.12
$1.65 \pm 0.07^{\text{d}}$	0.50 ± 0.05	16 ± 4	1.69	5.3 ± 0.6	39.09 ± 0.11
1.65 ± 0.07	0.66 ± 0.10	16 ± 4	1.69	4.2 ± 0.6	38.89 ± 0.12

^aOther parameters are $T_{\text{eff}} = 9000 \pm 500$ K, $\bar{V} = 16.6$, and a disk fraction of $21 \pm 5\%$ in V .

^bPeak X-ray luminosity during the 1983 outburst.

^cCorresponds to $2.3 \leq M_2 \leq 2.6 M_{\odot}$.

^dCorresponds to $M_2 = 0.5 M_{\odot}$.

of the black hole is in the range $2.7 \leq M_1 \leq 7.5 M_{\odot}$ (this is the mass range which assumes a main sequence secondary), which implies $3.1 \lesssim L_{\text{max}}/L_{\text{Edd}} \lesssim 8.7$. Unless the value of $E(B - V)$ has been seriously *underestimated* (larger values of $E(B - V)$ imply a closer system and a smaller value of L_{max}) and/or the inclination has been seriously *overestimated* (lower inclinations give a larger black hole mass and a larger value of L_{Edd}), the conclusion that $L_{\text{max}} > L_{\text{Edd}}$ seems unavoidable. Note that L_{max} was derived assuming the X-rays were emitted isotropically. If the X-ray emission was not isotropic, then possibly the accretion rate during the 1983 outburst could have been sub-Eddington. However, detailed model computations should be done, and such computations are beyond the scope of this paper.

6.3. Accretion Stability Considerations

As we discussed above, the temperature and radius of the secondary star are consistent with a $2.5 M_{\odot}$ star ≈ 393 Myr past the ZAMS. Mass transfer caused by expansion while on the main sequence is the so-called ‘‘Case A’’ phase (Kippenhahn & Weigert 1967). If 4U 1543-47 does indeed contain a main sequence A-type secondary the mass transfer will be stable since a star with a radiative envelope will shrink in response to mass loss (e.g. Soberman, Phinney, & van den Heuvel 1997). In general, a low-mass X-ray binary will be a transient system if its mass transfer rate

is below some critical value (e.g. van Paradijs 1996). The 1983 outburst released about 5.7×10^{45} ergs in X-rays (Chen, Schrader, & Livio 1997 and cited references), assuming $d = 9.0$ kpc. For an average outburst interval of 10.5 yr, this corresponds to an average X-ray luminosity of $\bar{L}_x = 1.7 \times 10^{37}$ ergs s⁻¹. The corresponding average mass transfer rate (assuming an efficiency of $0.2mc^2$ per gram of accreted matter; van Paradijs 1996) is 9.54×10^{16} g s⁻¹ = $1.51 \times 10^{-9} M_{\odot}$ yr⁻¹. Based on his model of the effects of X-ray irradiation on accretion disks, van Paradijs (1996) gives the dividing line between transient and persistent systems in the P_{orb} vs. \bar{L}_x plane as $\log \bar{L}_x = 35.8 + 1.07 \log P_{\text{orb}}$, where the orbital period is in hours. Systems below this line in the P_{orb} vs. \bar{L}_x plane are transient. With $P_{\text{orb}} = 26.95$ hours and $\bar{L}_x = 1.7 \times 10^{37}$ ergs s⁻¹, 4U 1543-47 is just below the dividing line between transients and persistent sources. Thus based on this quick analysis we conclude a main sequence secondary can produce stable mass transfer in a transient system.

7. Summary

We have measured the radial velocity curve of the secondary star in 4U 1543-47. The orbital period is $P = 1.123 \pm 0.008$ days and the K_2 velocity is $K_2 = 124 \pm 4$ km s⁻¹, which together give a mass function of $f(M) = 0.22 \pm 0.02 M_{\odot}$. The spectral type of the secondary is A2, and we see no emission

lines from the accretion disk and only a modest continuum flux from the disk in the B and V bands. The V and I light curves are ellipsoidal, which implies the A-star is the mass donor star and not a member of a triple system. Furthermore, the spectroscopic and photometric periods agree, and the relative phase of the radial velocity curve and the light curve is as expected. A model fit to the V and I light curves gives $24 \leq i \leq 36^\circ$ (3σ), with a lower limit of $i \geq 20^\circ$ and an upper limit of $i \leq 40^\circ$. The inferred radius, density, and temperature of the secondary are consistent with those of a $\approx 2.5 M_\odot$ main-sequence star which is ≈ 393 Myr past the ZAMS. If the secondary star is on the main sequence, then the primary mass is in the range $2.7 \leq M_1 \leq 7.5 M_\odot$. We conclude the compact object in 4U 1543-47 is very probably a black hole. Finally, we derive a distance of $d = 9.1 \pm 1.1$ kpc and a peak X-ray luminosity during the 1983 outburst of $L_{\max} = 3.6 \times 10^{39}$ ergs s^{-1} . The conclusion that the maximum X-ray luminosity of the 1983 outburst exceeded the Eddington luminosity is unavoidable ($3.1 \lesssim L_{\max}/L_{\text{Edd}} \lesssim 8.7$).

We thank George Jacoby for his donation of data, Richard Wade for his help with the synthetic spectra, Andrew King for useful discussions, and W. Niel Brandt for assistance with the ASCA archive. We are grateful to the staff of CTIO for the excellent support, in particular Srs. Mauricio Navarrete, Edgardo Cosgrove, Mauricio Fernandez, Manuel Hernandez, Patricio Ugarte, Hernan Tirdaro, & Daniel Maturana. Partial financial support for this work was provided by the National Science Foundation through a National Young Investigator grant to C. Bailyn, by the Smithsonian Institution Scholarly Studies Program to J. McClintock, and through a NASA funded grant administered by the American Astronomical Society to J. Orosz.

REFERENCES

- Avni, Y. 1978, in “Physics and Astrophysics of Neutron Stars and Black Holes,” eds. R. Giacconi & R. Ruffini (Amsterdam: North-Holland), 42
- Bailyn, C. D., et al. 1995a *Nature*, 374, 701
- Bailyn, C. D., Orosz, J. A., McClintock, J. E., & Remillard, R. A. 1995b, *Nature*, 378, 157
- Casares, J., & Charles, P. A. 1994, *MNRAS*, 271, L5
- Casares, J., et al. 1995, *MNRAS*, 276, L35
- Casares, J., et al. 1997, *New Astronomy*, 1, 299
- Chen, W., Schrader, C. R., & Livio, M. 1997, *ApJS*, in press (astro-ph/9707138)
- Chevalier, C. 1989, in “Two Topics in X-ray Astronomy”, 23rd ESLAB Symp., Bologna (ESA, Paris), page 341
- Filippenko, A. V., 1982, *PASP*, 94, 715
- Filippenko, A. V., Matheson, T., & Ho, L. C. 1995, *ApJ*, 455, 614
- Filippenko, A. V., et al. 1997, *PASP*, 109, 461
- Gray, D. F. 1992, “The Observations and Analysis of Stellar Photospheres” Cambridge Astrophysics Series #20, (Cambridge University Press, Cambridge)
- Greiner J., Predehl P., Harmon B.A., 1994, in “Proc. 2nd Compton Symposium”, Washington 1993, AIP 304, p. 314
- Guenther, D. B., Demarque, P., Kim, Y.-C., & Pinsonneault, M. H. 1992, *ApJ*, 387, 372
- Harmon, B. A., et al. 1992, *IAU Circular* #5504
- Horne, K. 1986, *PASP*, 98, 609
- Iglesias, C. A., & Rogers, F. J. 1996, *ApJ*, 464, 943
- Jaschek, C., & Jaschek, M. 1987, “The Classification of Stars”, (Cambridge University Press, Cambridge)
- Kippenhahn, R., & Weigert, A. 1967, *Zeitschrift für Astrophysik*, 66, 58
- Kitamoto, S. et al. 1984, *PASJ*, 36, 799
- Kolb, U., King, A. R., Ritter, H., & Frank, J. 1997, *ApJ*, 485, L33
- Landolt, A. U. 1992, *AJ*, 104, 340
- Li, F. K. et al. 1976, *ApJ*, 203, 187
- Marsh, T. R., Robinson, E. L., & Wood, J. H. 1994, *MNRAS*, 266, 137
- Matilsky, T. et al. 1972, *ApJ*, 174, L53
- McClintock, J. E., & Remillard, R. A. 1986, *ApJ*, 308, 110
- McClintock, J. E., & Remillard, R. A. 1990, *ApJ*, 350, 386
- Orosz, J. A., Bailyn, C. D., Remillard, R. A., McClintock, J. E., & Foltz, C. B. 1994, *ApJ*, 436, 848
- Orosz, J. A. 1996, Ph.D. Thesis, Yale University

- Orosz, J. A., Bailyn, C. D., McClintock, J. E., & Remillard, R. A. 1996, *ApJ*, 468, 380
- Orosz, J. A., & Bailyn 1997a, *ApJ*, 477, 876 (OB97)
- Orosz, J. A., & Bailyn 1997b, *ApJ*, 482, 1086
- Pederson, H. 1983, *ESO Messenger*, 34, 21
- Predehl, P. & Schmitt, J. H. M. M. 1995, *A&A*, 293, 889
- Press, W. H., Teukolsky, S. A., Vetterling, W. T., & Flannery, B. P. 1992, “Numerical Recipes in FORTRAN”, second edition, (Cambridge University Press, Cambridge)
- Pringle, J. E. 1985, in “Interacting Binary Stars”, eds. J. E. Pringle & R. A. Wade, Cambridge University Press, Cambridge, England, page 1
- Remillard, R. A., McClintock, J. E., & Bailyn, C. D. 1992, *ApJ*, 399, L145
- Remillard, R. A., Orosz, J. A., McClintock, J. E., & Bailyn, C. D. 1996, *ApJ*, 459, 226
- Soberman, G. E., Phinney, E. S., & van den Heuvel, E. P. J. 1997, *A&A*, in press (astro-ph/9703016)
- Stetson, P. B. 1987, *PASP*, 99, 191
- Stetson, P. B., Davis, L. E., & Crabtree, D. R. 1991, in “CCDs in Astronomy,” ed. G. Jacoby, ASP Conference Series, Volume 8, page 282
- Stetson, P. B. 1992a, in “Astronomical Data Analysis Software and Systems I,” eds. D. M. Worrall, C. Biemesderfer, & J. Barnes, ASP Conference Series, Volume 25, page 297
- Stetson, P. B. 1992b, in “Stellar Photometry—Current Techniques and Future Developments,” IAU Coll. 136, eds. C. J. Butler, & I. Elliot, Cambridge University Press, Cambridge, England, page 291
- Tanaka, Y., & Lewin, W. H. G. 1995 in “X-ray Binaries”, eds. W. H. G. Lewin, J. van Paradijs, & E. P. J. van den Heuvel, Cambridge University Press, Cambridge, England, page 126
- Tanaka, Y. & Shibazaki, N. 1996, *ARA&A*, 34, 607
- Tonry, J. & Davis, M. 1979, *AJ*, 84, 1511
- van der Hooft, F., et al. 1997, *A&A*, in press (astro-ph/9709151)
- van der Woerd, H., White, N. E., & Kahn, S. M. 1989, *ApJ*, 344, 320
- van Paradijs, J., & McClintock, J. E. 1995 in “X-ray Binaries”, eds. W. H. G. Lewin, J. van Paradijs, & E. P. J. van den Heuvel, Cambridge University Press, Cambridge, England, page 58
- van Paradijs, J. 1996, *ApJ*, 464, L139
- Wade, R. A., & Rucinski, S. M. 1985, *A&AS*, 60, 471
- Wade, R. A., & Horne, K. 1988, *ApJ*, 324, 411
- Zhang, S. N., et al. 1994, IAU Circular #6046